Biochemistry

Article

Cite This: *Biochemistry* 2018, 57, 5797−5806

pubs.acs.org/biochemistry

Conformational Dynamics of a Cysteine-Stabilized Plant Defensin Reveals an Evolutionary Mechanism to Expose Hydrophobic Residues

Luciana E.S.F. Machado,[†,‡] Viviane S. De Paula,[†] Yulia Pustovalova,[‡] Irina Bezsonova,[‡] Ana Paula Valente,[†] Dmitry M. Korzhnev,[*,‡] and Fabio C. L. Almeida[*,†]

[†]Centro Nacional de Ressonância Magnética Nuclear de Macromoléculas, Instituto de Bioquímica Médica e Centro Nacional de Biologia Estrutural e Bioimagem (CENABIO), Universidade Federal do Rio de Janeiro, Rio de Janeiro 21941-902, Brazil

[‡]Department of Molecular Biology and Biophysics, University of Connecticut Health Center, Farmington, Connecticut 06030, United States

Supporting Information

ABSTRACT: Sugar cane defensin 5 (Sd5) is a small antifungal protein, whose structure is held together by four conserved disulfide bridges. Sd5 and other proteins sharing a cysteine-stabilized α-β (CS$\alpha\beta$) fold lack a regular hydrophobic core. Instead, they are stabilized by tertiary contacts formed by surface-exposed hydrophilic and hydrophobic residues. Despite excessive cross-links, Sd5 exhibits complex millisecond conformational dynamics involving all secondary structure elements. We used Carr−Purcell−Meiboom−Gill (CPMG) NMR relaxation dispersion (RD) measurements performed at different temperatures and denaturant concentrations to probe brief excursions of Sd5 to a sparsely populated "excited" state. Temperature-dependent CPMG RD experiments reveal that the excited state is enthalpically unfavorable, suggesting a rearrangement of stabilizing contacts formed by surface-exposed side chains and/or secondary structure, while the experiments performed at different denaturant concentrations suggest a decrease in accessible surface area of Sd5 in the excited state. The measured backbone ^{15}N chemical shift changes point to a global conformational rearrangement such as a potential α- to β-transition of the Sd5 α-helix or other major secondary structure reorganization and concomitant conformational changes in other parts of the protein. Overall, the emerging picture of Sd5 dynamics suggests this protein can populate two alternative well-ordered conformational states, with the excited conformer being more compact than the native state and having a distinct secondary structure and side-chain arrangements. The observation of an energetically unfavorable yet more compact excited state reveals a remarkable evolution of the CS$\alpha\beta$ fold to expose and reorganize hydrophobic residues, which enables the creation of versatile binding sites.

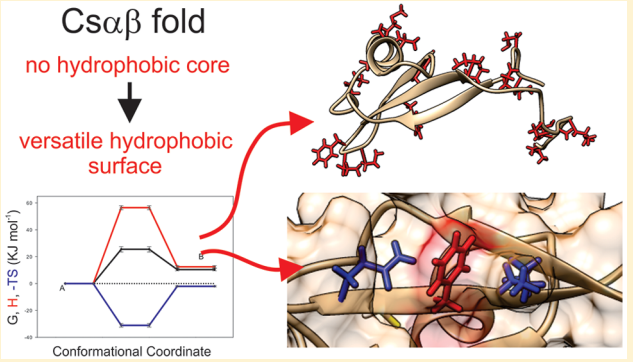

The immune system is central to evolution of life on Earth. Defensins are the main component of the most ancestral innate immune system. The development of an adaptive immune system came later, at around 550 million years ago (mya) with the emergence of jawed vertebrates.[1,2] Evolutionary analysis reveals a common ancestor of defensins, which dates back to ca. 100 mya.[3−5] The plant defensin fold, which is often referred to as cysteine-stabilized α-β motif (CS$\alpha\beta$), consists of a β-sheet formed by 3 antiparallel β-strands and an α-helix. Also, defensins and other protein components of the innate and adaptive immune systems such as cytokines and ion blockers are disulfide-stabilized. Excessive disulfide cross-links help maintain the CS$\alpha\beta$ fold and enable a high primary sequence diversity in the defensin family with cysteines being the only highly conserved residues.[4] Such a sequence variability also explains functional diversity among defensins and helps individual defensins fulfill multiple functions.[6] Because of the high primary sequence diversity in the defensin family, evolution of the defensin fold remains elusive.[3,7,8]

Defensins are ancestral proteins displaying antimicrobial activity against fungi or bacteria found in complex organisms such as insects, plants, avian, and mammals.[9] These small thermally stable proteins share a cationic and amphipathic character, which allows them to interact with microbial membranes.[10,11] Despite a key role played by defensins in the innate immune system, molecular mechanisms of their action are not yet fully understood.

Growing evidence suggests that plant defensins interact with fungal cell membranes followed by their internalization and binding to intracellular targets.[12,13] One known membrane

Received: July 15, 2018
Revised: September 10, 2018
Published: September 12, 2018

DOI: 10.1021/acs.biochem.8b00753
Biochemistry 2018, 57, 5797−5806

target of defensins such as radish defensin (RsAPV2), insect defensin heliomicin, *Pisum sativum* defensin 1 (Psd1),[14] and sugar cane defensin 5 (Sd5) is fungal glucosylcerebroside CMH.[3,13,15,16] Despite sharing a similar fold, Psd1 and Sd5 interact with CMH via different interfaces,[13,15] suggesting that the binding site for CMH is not conserved in the defensin family. In addition to targeting fungal membranes, defensins recognize intracellular targets such as cyclins.[12,17] Unlike plant defensins, human defensins interact with bacterial membranes and play a role in antimicrobial defense, while also mediating an interplay between the innate and adaptive immune systems.[18]

Because defensins are stabilized by an unusually high number of disulfides bonds, it was implicit that they possess a restricted backbone mobility. Surprisingly, recent NMR studies of the defensin dynamics[13,15,18] revealed that these heavily cross-linked small proteins exhibit extensive conformational dynamics. For instance, the Psd1 plant defensin exhibits millisecond time-scale dynamics in the $\beta1/\alpha1$ loop,[13] while the Sd5 defensin studied here shows millisecond dynamics involving all secondary structure elements.[15] Previous reports suggest that variations in the membrane binding properties among plant defensins can be attributed to differences in their conformational dynamics, which needs to be taken into account when considering membrane recognition. Therefore, detailed studies of the defensin dynamics may provide important insights into specificities of different defensins toward their numerous targets, including bacterial lipid II receptor, fungal phospholipids, and sphingolipids,[19] which cannot be explained from defensin structure alone.[20]

The extensive micro- to millisecond conformational exchange displayed by defensins can be attributed to transient interconversions between the ground native state and energetically less favorable "excited" state(s). Previous works have shown that transitions to such sparsely populated conformers are implicated in many aspects of protein function.[21−25] Carr−Purcell−Meiboom−Gil relaxation dispersion (CPMG RD) methods provide versatile tools to probe thermodynamics and kinetics of such conformational equilibria and elucidate structural properties of excited states on the protein energy landscape.[26,27]

Here we use ^{15}N CPMG RD methods to study the conformational exchange of the Sd5 defensin, which involves millisecond time-scale transitions to a low-populated excited state. The native state of Sd5 is cross-linked by four disulfide bonds and does not have a typical hydrophobic core. Instead, the most prevalent tertiary interactions in the CS$\alpha\beta$ fold are the contacts mediated by surface-exposed polar and hydrophobic side chains. ^{15}N CPMG RD measurements performed as a function of temperature and denaturant concentration reveal Sd5 transitions to energetically unfavorable yet more compact excited state with a distinct secondary structure arrangement. Thus, the observed ^{15}N chemical shift changes are consistent with a potential α- to β-transition of the Sd5 α-helix or other major secondary structure reorganization and concomitant conformational changes in other parts of the protein. Such a transition must be accompanied by rearrangement of the Sd5 surface-exposed side chains, potentially creating additional binding sites. Overall, extensive dynamics of the Sd5 CS$\alpha\beta$ fold reveal an evolutionary mechanism to expose and rearrange hydrophobic residues, which enables individual defensins to fulfill multiple functions and endows functional diversity to the defensin family.

MATERIAL AND METHODS

Protein Expression and Purification. The uniformly ^{15}N-labeled plant defensin Sd5 was expressed and purified as described previously.[15] In brief, a gene encoding Sd5 (residues 1−71) was subcloned into a pET28a vector using NdeI and *Bam*HI restriction sites. Protein was expressed in *E. coli* BL21(DE3) cells transformed with the Sd5 plasmid. The culture was grown at 37 °C in 1 L of minimal M9 media containing 1 g/L $^{15}NH_4Cl$ as a sole source of nitrogen. Protein expression was induced at OD_{600} = 0.7 with 1 mM IPTG. Cells were harvested 5 h after induction by centrifugation at 6037.2*g* for 10 min at 4 °C, resuspended in buffer A (20 mM sodium phosphate buffer, pH 7.5, 500 mM NaCl, 10 mM imidazole), and lysed by sonication. The lysate was clarified by centrifugation at >6000*g* for 30 min at 4 °C. The supernatant was incubated with Ni^{2+} resin (30 min at 4 °C), and then after an extensive wash with buffer A, the protein was eluted with buffer B (20 mM sodium phosphate buffer, pH 7.5, 500 mM NaCl, 500 mM imidazole). His-tag was cleaved with thrombin at room temperature overnight. The protein was further purified on a reversed-phase C18 column with a gradient of acetonitrile (0 to 45%) in the buffer containing 0.1% TFA. After purification, the ^{15}N-labeled Sd5 protein was lyophilized and then resuspended at 1 mM concentration in an NMR buffer containing 20 mM sodium phosphate buffer, pH 6.0, 90% H_20/10% ^2H_2O.

^{15}N Relaxation Dispersion Measurements. ^{15}N Carr−Purcell−Meiboom−Gill relaxation dispersion (CPMG RD) profiles for ^{15}N-labeled Sd5 were recorded on Agilent VNMRS spectrometers at four temperatures (15, 20, 25, and 30 °C) and two magnetic fields (14.1 and 18.8 T) using the constant relaxation time ^{15}N CPMG pulse experiment with ^{1}H continuous wave (CW) decoupling during the CPMG element.[28] In addition, the experiments recorded at 25 °C were repeated at 4 urea concentrations (0, 0.3, 0.6, and 1 M). All ^{15}N CPMG RD experiments were performed at a constant relaxation time period, T_{relax}, of 40 ms and with CPMG frequencies $\nu_{CPMG} = 1/(2\tau)$ ranging from 25 to 1000 Hz, where τ is the delay between the consecutive 180° refocusing pulses of the ^{15}N CPMG pulse train. Relaxation dispersion profiles $R_{2,eff}(\nu_{CPMG})$ were calculated from peak intensities (I) in a series of two-dimensional (2D) ^{1}H−^{15}N correlation spectra recorded at different CPMG frequencies, ν_{CPMG}, using the following equation: $R_{2,eff}(\nu_{CPMG}) = -1/T_{relax}\ln(I/I_0)$, where I is the signal intensity in spectra collected at T_{relax} = 40 ms and I_0 is the signal intensity in the reference spectrum recorded at T_{relax} = 0. Uncertainties in $R_{2,eff}$ rates were estimated from peak intensities in repeat spectra collected at two or more CPMG frequencies. In cases where estimated uncertainties were less than 2% of the $R_{2,eff}$ value, the minimal uncertainty of 2% was assumed.

Fitting of Temperature-Dependent CPMG RD Data. ^{15}N CPMG RD data for multiple amide groups of Sd5 recorded at 4 temperatures and 2 magnetic fields were fit together to a model of two-state exchange between the ground state (A) and a low-populated excited state (B) by minimization of the following $\chi^2(\zeta)$ target function:

$$\chi^2(\zeta) = \sum \frac{(R_{2,eff}^{clc}(\zeta) - R_{2,eff}^{exp})^2}{(\Delta R_{2,eff}^{exp})^2} \quad (1)$$

DOI: 10.1021/acs.biochem.8b00753
Biochemistry 2018, 57, 5797−5806

where $R_{2,\mathrm{eff}}^{\mathrm{exp}}$ and $\Delta R_{2,\mathrm{eff}}^{\mathrm{exp}}$ are experimental effective relaxation rates and their uncertainties, respectively, $R_{2,\mathrm{eff}}^{\mathrm{clc}}(\zeta)$ is the model relaxation rate obtained by the numerical solution of Bloch−McConnell equations,[29] $\zeta = \{\chi_1, ..., \chi_{n_{\mathrm{par}}}\}$ is a set of adjustable model parameters, n_{par} is the number of adjustable parameters. Summation in eq 1 is over the number of experimental data points, n_{dat}. The data fitting was performed using an in-house software cpmg_fit[30,31] under the assumptions that (i) all residues in Sd5 are involved in the same global exchange process, (ii) intrinsic relaxation rates, $R_{2,0}$, are the same in states A and B, (iii) chemical shift differences between states, $\Delta\varpi_{\mathrm{BA}}$, are independent of temperature, and (iv) populations of the exchanging states and rates of transitions between states follow the Boltzmann distribution and Eyring equation:

$$p_{\mathrm{B}}/p_{\mathrm{A}} = \exp(-\Delta G_{\mathrm{BA}}/(RT)) \quad (2)$$

$$k_{\mathrm{B}\to\mathrm{A}} = (k_{\mathrm{B}}\kappa\cdot T/\hbar)\cdot\exp(-\Delta G^{\ddagger}_{\mathrm{BA}}/(R\cdot T)) \quad (3)$$

where $\Delta G_{\mathrm{BA}} = \Delta H_{\mathrm{BA}} - T\Delta S_{\mathrm{BA}}$ is the free energy difference between states B and A, $\Delta G^{\ddagger}_{\mathrm{BA}} = \Delta H^{\ddagger}_{\mathrm{BA}} - T\Delta S^{\ddagger}_{\mathrm{BA}}$ is the activation free energy, ΔH_{BA}, ΔS_{BA}, $\Delta H^{\ddagger}_{\mathrm{BA}}$, and $\Delta S^{\ddagger}_{\mathrm{BA}}$ are equilibrium and activation entropies and enthalpies, respectively, $\hbar$, k_{B}, and R are the Planck's, Boltzmann's, and universal gas constants, respectively, and κ is a transmission coefficient. $\kappa = 1.6 \times 10^{-7}$ was used, which was suggested for the protein folding process.[32−34] The set of adjustable model parameters in the global two-state exchange model included ΔH_{BA}, ΔS_{BA}, $\Delta H^{\ddagger}_{\mathrm{BA}}$, and $\Delta S^{\ddagger}_{\mathrm{BA}}$, chemical shift differences between states for all residues, $\Delta\varpi_{\mathrm{BA}}$, and intrinsic relaxation rates, $R_{2,0}$, for all residues, temperatures, and magnetic fields.

As an alternative approach, ^{15}N CPMG RD data for the same set of residues recorded at 2 magnetic fields were analyzed independently for each temperature to extract the population of the minor state, p_{B}, exchange rate constant, $k_{\mathrm{ex}} = k_{\mathrm{A}\to\mathrm{B}} + k_{\mathrm{B}\to\mathrm{A}}$, $\Delta\varpi_{\mathrm{BA}}$ values for all residues, and $R_{2,0}$ values for all residues and magnetic fields. Equilibrium and activation parameters, ΔH_{BA}, ΔS_{AB} $\Delta H^{\ddagger}_{\mathrm{BA}}$, and $\Delta S^{\ddagger}_{\mathrm{BA}}$, were then obtained from linear fits of $\ln(p_{\mathrm{B}}/p_{\mathrm{A}})$ vs $1/T$ and $\ln(k_{\mathrm{B}\to\mathrm{A}})$ vs $1/T$. (See eqs 2 and 3.)

Fitting of Urea-Dependent CPMG RD Data. ^{15}N CPMG RD data recorded as a function of urea concentration were analyzed using a procedure similar to that described for the temperature-dependent data. CPMG RD data for multiple amide groups obtained at 4 urea concentrations and 2 magnetic fields were fit together to a model of two-state exchange between the ground state A and excited state B assuming that (i) all residues in Sd5 are involved in the same exchange process, (ii) intrinsic $R_{2,0}$ rates are the same for both states, (iii) chemical shift differences between states, $\Delta\varpi_{\mathrm{BA}}$, are independent of urea concentration, and (iv) dependences of populations of exchanging states and exchange rates on urea concentration, [urea], are given by eqs 2 and 3 with $\Delta G_{\mathrm{BA}} = \Delta G_{\mathrm{BA},0} - m_{\mathrm{BA}}$ [urea] and $\Delta G^{\ddagger}_{\mathrm{BA}} = \Delta G^{\ddagger}_{\mathrm{BA},0} - m^{\ddagger}_{\mathrm{BA}}$ [urea], where $\Delta G_{\mathrm{BA},0}$ is the free energy difference between states at [urea] = 0, $\Delta G^{\ddagger}_{\mathrm{BA},0}$ is the activation free energy at [urea] = 0, m_{BA} is the m value difference between states, and $m^{\ddagger}_{\mathrm{BA}}$ is the activation m value. The set of adjustable model parameters of the global two-state exchange model included $\Delta G_{\mathrm{BA},0}$, $\Delta G^{\ddagger}_{\mathrm{BA},0}$, m_{BA}, $m^{\ddagger}_{\mathrm{BA}}$, $\Delta\varpi_{\mathrm{BA}}$ values for all residues, and $R_{2,0}$ for all residues, urea concentrations, and magnetic fields.

Alternatively, ^{15}N CPMG RD data for all residues recorded at 2 magnetic fields were fit independently for each urea concentration to extract p_{B}, k_{ex}, $\Delta\varpi_{\mathrm{BA}}$, and $R_{2,0}$ values. The equilibrium and activation parameters, $\Delta G_{\mathrm{AB},0}$, $\Delta G^{\ddagger}_{\mathrm{BA},0}$, m_{BA}, and $m^{\ddagger}_{\mathrm{BA}}$, were then obtained from linear fits of $\ln(p_{\mathrm{B}}/p_{\mathrm{A}})$ vs [urea] and $\ln(k_{\mathrm{B}\to\mathrm{A}})$ vs [urea]. (See eqs 2 and 3.)

Quality of Data Fits. The quality of data fits by global two-state exchange models was assessed by comparing the resulting values of $\chi^2(\zeta)$ target function (eq 1) to the number of degrees of freedom (DF) of the model DF = $n_{\mathrm{dat}} - n_{\mathrm{par}}$. In the case of normally distributed and uncorrelated experimental errors $\Delta R_{2,\mathrm{eff}}^{\mathrm{exp}}$, $\chi^2(\zeta)$ in its minimum follows χ^2 distribution with degrees of freedom. At a large DF, χ^2 distribution converges to a normal distribution centered at DF with the standard deviation of $(2\cdot\mathrm{DF})^{1/2}$. Therefore, global fits of ^{15}N CPMG RD data should result in $\chi^2(\zeta)$ of the order of DF provided that (i) experimental errors $\Delta R_{2,\mathrm{eff}}^{\mathrm{exp}}$ are estimated correctly and (ii) the model adequately fits the data. The values of $\chi^2(\zeta)$ target functions obtained in global fits of CPMG RD data are shown in Table S1. $\chi^2(\zeta)$ of the order or less than DF were obtained in all data fits, showing that the model of global two-state conformational exchange involving multiple Sd5 residues fits the data to within experimental uncertainties.

Previously, it was shown that at typical uncertainties of experimental $R_{2,\mathrm{eff}}$ rates (2% or more) ^{15}N CPMG RD data for a single amide group are not sufficient to effectively discriminate between the two-state and more complex (e.g., three-state) conformational exchange models.[35] Such discrimination is only possible based on global fits of CPMG RD data obtained for multiple residues/nuclei/spin coherences, preferably at different sets of experimental conditions (e.g., temperatures).[35,36] A large discrepancy between $\chi^2(\zeta)$ obtained in the global two-state CPMG RD data fit and the sum of $\chi^2(\zeta)$ ($\Sigma\chi^2$) obtained in data fits for individual amide groups can, therefore, provide an indication that a more complex model should be considered. Table S1 shows the comparison of $\chi^2(\zeta)$ values obtained in global fits of CPMG RD data with the sum of per-residue $\chi^2(\zeta)$ values ($\Sigma\chi^2$). In all cases, a good agreement between the two values is observed ($\chi^2(\zeta)/\Sigma\chi^2$ ratio of up to 1.5), suggesting that the use of a more complex exchange model is not justified.

Neighbor-corrected intrinsically disordered protein (IDP) chemical shifts for the Sd5 primary sequence were calculated as described in Tamiola et al., 2010[37] using the server http://nmr.chem.rug.nl/ncIDP. Random coil chemical shifts were calculated as described in Schwarzinger et al.[38,39] ($\Delta\varpi^{\mathrm{rc}}$).

RESULTS

Sd5 Undergoes a Global Millisecond Time-Scale Conformational Exchange. Previous studies by our group demonstrated that sugar cane defensin 5 (Sd5) exhibits complex millisecond time-scale dynamics involving all secondary structure elements,[15] as illustrated in Figure 1A. Global rearrangement of Sd5 can be attributed to a conformational equilibrium between the lowest energy native state and less favorable excited conformational state(s). To assess thermodynamics and kinetics of these interconversions and probe the structure of the excited state(s), we have collected ^{15}N single-quantum (SQ) Carr−Purcell−Meiboom−Gill relaxation dispersion (CPMG RD) data for Sd5 at two magnetic field strengths (14.1 and 18.8 T) as a function of temperature and denaturant concentration. Figure 1B,C shows examples of temperature (plot B) and denaturant (plot C)

DOI: 10.1021/acs.biochem.8b00753
Biochemistry 2018, 57, 5797−5806

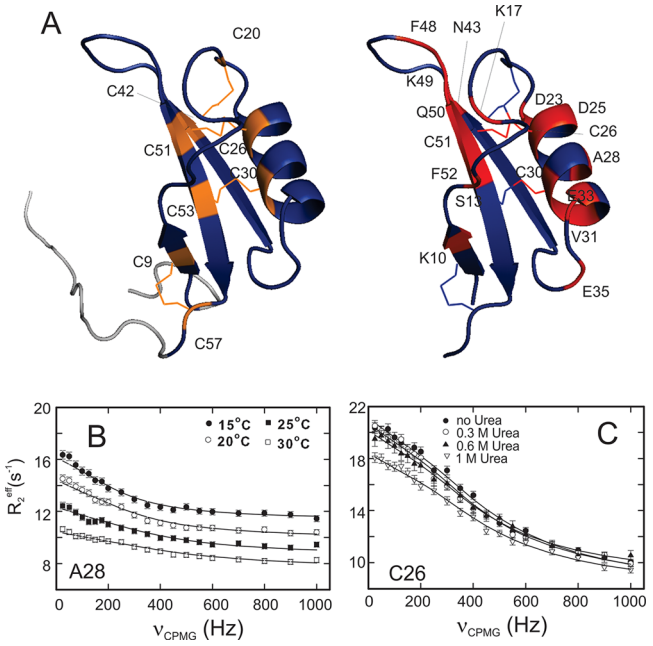

Figure 1. ^{15}N CPMG relaxation dispersion profiles for Sd5. (A) Ribbon diagram of Sd5 showing in the left the 4 disulfide bonds (orange), the N- and C-terminal flexible tails (gray). The right images depicts the 17 residues exhibiting a millisecond time-scale conformational exchange (red) identified in our previous model-free analysis of ^{15}N relaxation data.[15] (B, C) Examples of the backbone ^{15}N CPMG RD profiles for selected Sd5 residues recorded at 18.8 T magnetic field as a function of temperature (B) and urea concentration (C).

dependent ^{15}N CPMG RD profiles (18.8 T field) for selected Sd5 residues, with additional examples shown in Figure S1.

Conformational Exchange in Sd5 Is Described by a Two-State Mechanism. First, we asked whether the conformational equilibrium in Sd5 is described by a model of global two-state exchange between the ground native state (A) and a single low-populated excited state (B), or a more complex exchange model is required to fit ^{15}N CPMG RD data. To answer this question, we evaluated how well the two-state model can simultaneously fit ^{15}N CPMG RD profiles for multiple Sd5 residues obtained at different temperatures and denaturant concentrations. The top part of Table S1 shows the values of $\chi^2(\zeta)$ target function (eq 1) obtained in global fits of CPMG RD data for Sd5 amide groups at individual temperatures and urea concentrations, while the bottom part summarizes the results of global fits where the data for all temperatures and/or denaturant concentrations were analyzed together. All fits resulted in $\chi^2(\zeta)$ of the order or less than the number of degrees of freedom of the model, suggesting that the two-state exchange model adequately fits the data according to χ^2 statistics criterion and that the use of more complicated global three-state models in our case is not justified.

Although we have assumed fairly stringent errors for $R_{2,\mathrm{eff}}$ rates measured in the CPMG experiment, there is a finite possibility that the low $\chi^2(\zeta)$ values obtained in data fits by the two-state exchange model (Table S1) result from overestimated experimental uncertainties, $\Delta R_{2,\mathrm{eff}}$. To exclude this possibility, we compared (i) $\chi^2(\zeta)$ values obtained in the global ^{15}N CPMG RD data fits with (ii) the sum of $\chi^2(\zeta)$ ($\Sigma\chi^2$) obtained in data fits for individual residues (Table S1). A good agreement between global $\chi^2(\zeta)$ and $\Sigma\chi^2$ would suggest that the global two-state model adequately fits the data. Conversely, an increase in global $\chi^2(\zeta)$ relative to $\Sigma\chi^2$ would indicate that a more complex model is needed.[31] The moderate (up to 1.5 fold) increase in $\chi^2(\zeta)$ obtained in global fits of temperature- and denaturant-dependent CPMG data as compared to $\Sigma\chi^2$ is much smaller than those obtained in previous ^{15}N CPMG RD studies of proteins involved in global multistate exchange processes (2 times or higher),[30,40] suggesting that the use of a more complex conformational exchange model for Sd5 is not justified.

Temperature Dependence of Exchange Parameters Reveals an Ordered Excited State. CPMG RD data analysis allows extraction of the two-state exchange parameters, including population of the minor state, p_B, exchange rate constant, $k_{ex} = k_{A\to B} + k_{B\to A}$, and absolute values of chemical shift differences between the ground and excited states, $|\Delta\varpi_{AB}|$. The analysis of temperature dependences of equilibrium ($K_{eq} = p_B/p_A$) and rate ($k_{B\to A}$) constants provides equilibrium and activation entropies and enthalpies for the exchange process, ΔH_{BA}, ΔS_{BA}, $\Delta H^{\ddagger}_{BA}$, and $\Delta S^{\ddagger}_{BA}$. To determine these parameters for the exchange process in Sd5, we used two alternative approaches. In the first approach, ΔH_{BA}, ΔS_{BA}, $\Delta H^{\ddagger}_{BA}$, and $\Delta S^{\ddagger}_{BA}$ were used as adjustable parameters in the global fit of ^{15}N CPMG RD data for multiple residues measured at different temperatures (Materials and Methods). In the second approach, ^{15}N CPMG RD data for multiple residues were fit with adjustable p_B and k_{ex} at each individual temperature. Equilibrium and activation entropies and enthalpies were then obtained from linear fits of $\ln(K_{eq})$ and $\ln(k_{B\to A})$ vs $1/T$ (eqs 2 and 3).

Figure 2 shows temperature dependences of p_B and k_{ex} (plots A and C), the vaṅt Hoff and Arrhenius plots, $\ln(K_{eq})$ and $\ln(k_{B\to A})$ vs $1/T$ (plots B and D), and thermodynamic parameters (i) obtained from plots B and D and (ii) extracted from the global fit of temperature-dependent ^{15}N CPMG RD data plotted in a form of Sd5 energy landscape (plot E). Figure 2E shows the energy landscape of Sd5 at 25 °C, depicting the free energy (G), enthalpic (H), and entropic (TS) contributions to G along the pathway of the exchange process obtained by the two approaches described above, illustrating robustness of the extracted thermodynamic parameters.

The obtained thermodynamic parameters (Figure 2E; Table S2) suggest that the free energy difference between the excited and ground states of Sd5, ΔG_{BA} = 10.4 kJ/mol at 25 °C, is mostly accounted for by a higher enthalpy of the excited state. Thus, the enthalpy difference between states contributes ~85% of the free energy change (ΔH_{BA} of 10.8−12.5 kJ/mol), while the entropic term contributes only ~15% of the change ($T\Delta S_{BA}$ of 0.39−2.01 kJ/mol). The energy profiles shown in Figure 2E are in striking contrast with those reported for order/disorder transitions of small protein domains obtained by CPMG RD methods,[30,31,40] where a relatively small free energy difference ΔG_{BA} ~ 10.9 kJ/mol results from large mutually compensating entropic and enthalpic terms. These opposing contributions stem from classic entropy−enthalpy compensation upon protein folding due to a decrease in configurational entropy of the polypeptide chain compensated by the formation of favorable enthalpic contacts in the native state and an increase in solvent entropy upon the polypeptide chain dehydration.[41] Neither of these is observed for Sd5, where the excited state is enthalpically less stable, presumably due to a less optimal side-chain arrangement and/or reorganization of secondary structure, yet entropically similar

DOI: 10.1021/acs.biochem.8b00753
Biochemistry 2018, 57, 5797−5806

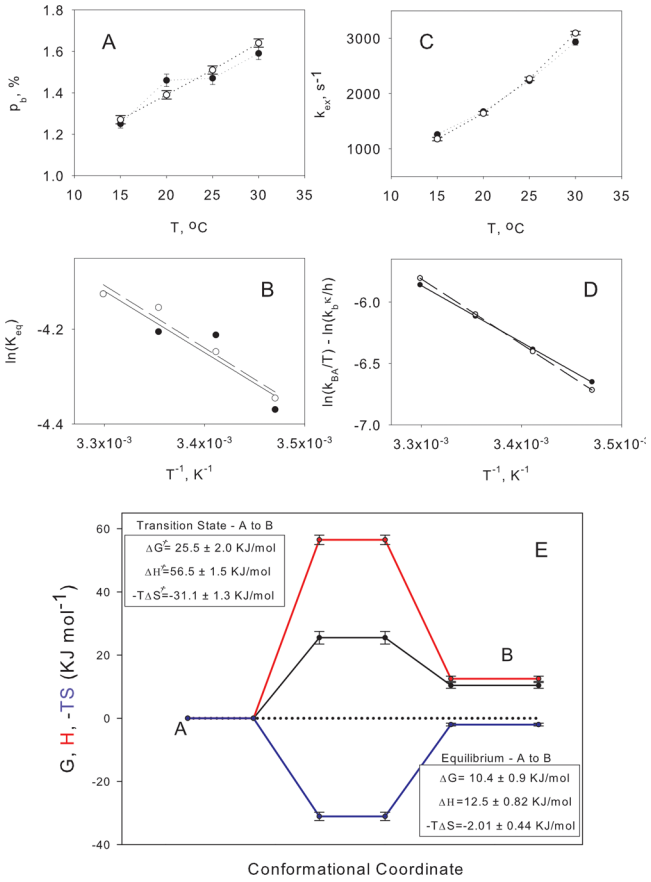

Figure 2. Kinetic and thermodynamic parameters derived from relaxation dispersion experiments. Temperature dependences of population of the excited state p_B (A) and exchange rate constant k_{ex} (C). The values of p_B and k_{ex} obtained from CPMG RD data fits at individual temperatures are shown by filled circles and dashed lines; the values obtained from the global fit of the data measured at different temperatures are shown by open circles and dashed lines. Van't Hoff plot of $\ln(K_{eq})$ vs $1/T$ (B) and Eyring plot $[\ln(k_{B\to A}/T) - \ln(k_b\kappa/\hbar)]$ vs $1/T$ (D) generated using p_B and k_{ex} obtained from data fits at individual temperatures (filled circles and solid lines) and global fit of the data measured at different temperatures (open circles and dashed lines). (E) Free energy (G, black line), enthalpy (H, red line), and entropic contribution (TS, blue line) to the free energy along the pathway of global conformational exchange process in Sd5 calculated at 25 °C. Here we show thermodynamic parameters obtained from the global fit of CPMG RD data measured at different temperatures. Thermodynamic parameters resulting from p_B and k_{ex} obtained at individual temperatures can be found in Table S2. (See Materials and Methods for details.)

to the populated ground state. This result points to a global conformational rearrangement of the Sd5 that involves transitions to a well-ordered excited state.

Temperature dependence of the process kinetics reveals that the barrier for transition between states is largely enthalpic. (That is, $\Delta G^{\ddagger}_{AB}$ of 25.5 kJ/mol consists of 49.2−56.5 kJ/mol $\Delta H^{\ddagger}_{AB}$ and 23.6−31.1 kJ/mol $T\Delta S^{\ddagger}_{AB}$ contributions.) The dominant enthalpic contribution to the transition state energy likely results from breaking/rearrangement of a secondary structure and/or tertiary contacts mediated by surface-exposed side chains. An entropic contribution to the barrier height may result from an increased flexibility of the transition state.

Denaturant *m* Values Reveal a Compact Excited State. To gain additional insights into properties of the excited state, we have studied the effect of subdenaturation concentrations of urea on thermodynamics and kinetics of conformational exchange in Sd5. CPMG RD measurements performed as a function of denaturant concentration allow extraction of the m value difference between the excited and native states, $m_{BA} = m_B - m_A$, and activation m values, $m^{\ddagger}_{AB}$ and $m^{\ddagger}_{BA}$, describing linear dependencies of equilibrium and activation free energies of the process on denaturant concentration. The m values for urea denaturation ($m_{DN} = m_D - m_N = -\partial(\Delta G_{DN})/\partial[\text{urea}]$, where N and D denote native and denatured states, respectively) are very informative because they correlate with protein surface exposure.[42] Thus, the m value expected for protein unfolding $m_{DN} = m_D - m_N$ is always positive, reflecting a decrease in protein stability ($\Delta G_{DN} = G_D - G_N$) with an increasing denaturant concentration and a concomitant increase in protein accessible surface area upon unfolding.[42] The urea unfolding m values, m_{DN}, in the range from 0.25 to 1.25 kcal/mol/M (1.0−5.2 kJ/mol/M) (where M denotes moles of urea) have been reported for small proteins under 100 amino acid residues.[42]

Figure 3A,B shows urea dependences of population of the excited state, p_B, and exchange rate constant, k_{ex}, obtained from the analysis of CPMG RD data (Figure 1C). Remarkably, the population of the minor state, p_B, decreases with urea concentration (from 0 to 1 M), suggesting destabilization of the excited state relative to the ground state in the presence of an increasing amount of denaturant. This is opposite to what is expected for protein unfolding where the population of less ordered states with a higher accessible surface area is expected to increase with an addition of denaturant. On the other hand, the exchange rate constant $k_{ex} = k_{B\to A} + k_{A\to B}$ (dominated by $k_{B\to A}$ rate) remains essentially unchanged with denaturant concentration, suggesting little change in solvent exposure between the excited and transition states.

Similar to the analysis of temperature-dependent CPMG RD data, we estimated equilibrium and activation m values for the exchange process from the analysis of denaturant-dependent CPMG data by the two approaches: (i) by using m_{BA} and $m^{\ddagger}_{BA}$ as adjustable parameters in the global fit of CPMG RD data recorded at different urea concentrations and (ii) by extracting p_B and k_{ex} for each urea concentration independently and then obtaining m_{BA} and $m^{\ddagger}_{BA}$ from linear fits of $\ln(K_{eq})$ and $\ln(k_{B\to A})$ vs [urea] (where $K_{eq} = p_B/p_A$, $k_{B\to A} = p_B k_{ex}$) (Figure 3C,D). A good agreement between the results of the two methods illustrate robustness of our m value estimates (Figure 3E).

Figure 3E shows the m value profile along the pathway of exchange process in Sd5. (See also Table S3.) Sd5 transition to the excited state is accompanied by a decrease in m value with $m_{BA} = m_B - m_A$ ranging from −660 ± 89 to −737 ± 18 J mol^{-1} M^{-1}. This is a relatively small but statistically significant change, suggesting that the excited state of Sd5 has a less accessible surface area than the ground native state, presumably due to rearrangement of surface-exposed side chains into cluster(s), leading to the burial of exposed hydrophobic groups (see below). On the other hand, the m value difference between the transition and excited states ($m^{\ddagger}_{BA}$) is close to zero (−160 ± 41 J mol^{-1} M^{-1}), suggesting that the Sd5 rearrangement accompanied by the m value increase on the way from the excited to the native state occurs after the rate-limiting step.

^{15}N Chemical Shift Changes Suggest a Major Reorganization of Secondary Structure. Figure 4 shows

DOI: 10.1021/acs.biochem.8b00753
Biochemistry 2018, 57, 5797−5806

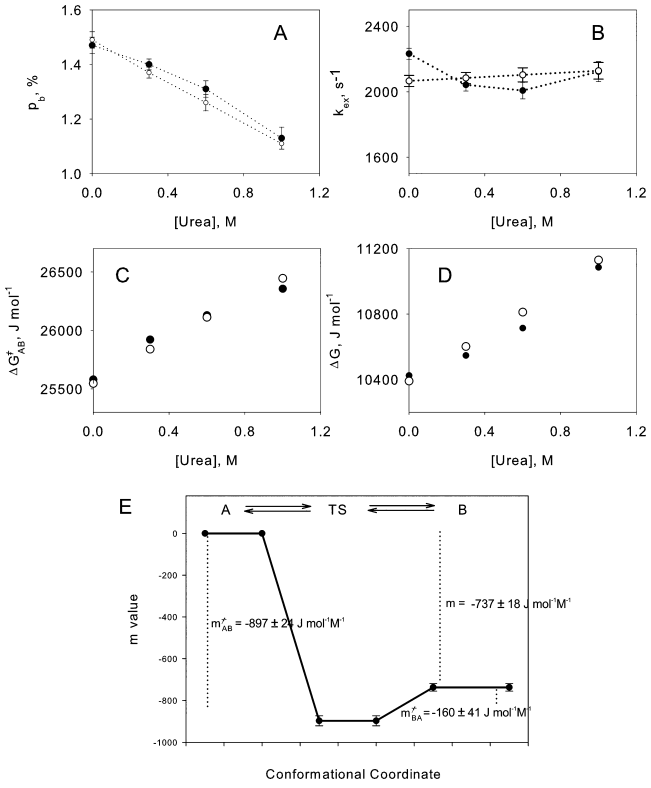

Figure 3. Effect of subdenaturation concentrations of urea on conformational exchange in Sd5. (A) Population of the excited state p_B and (B) exchange rate constant k_{ex} as a function of urea concentration: open circles show the values obtained in the global fit of CPMG RD data at different urea concentrations, and filled circles show the values obtained in individual data fits performed independently at each urea concentration. (C) Equilibrium (ΔG_{BA}) and (D) activation ($\Delta G^{\ddagger}_{BA}$ and $\Delta G^{\ddagger}_{AB}$) free energies obtained from p_B and k_{ex} shown on plots A and B shown as a function of urea concentration. (E) m value profiles along the pathway of exchange process in Sd5 obtained from the global fit of CPMG RD data at different urea concentrations with adjustable m_{BA} and $m^{\ddagger}_{BA}$. The parameters obtained from data fits at individual urea concentrations are shown in Table S3. (See Materials and Methods for details.)

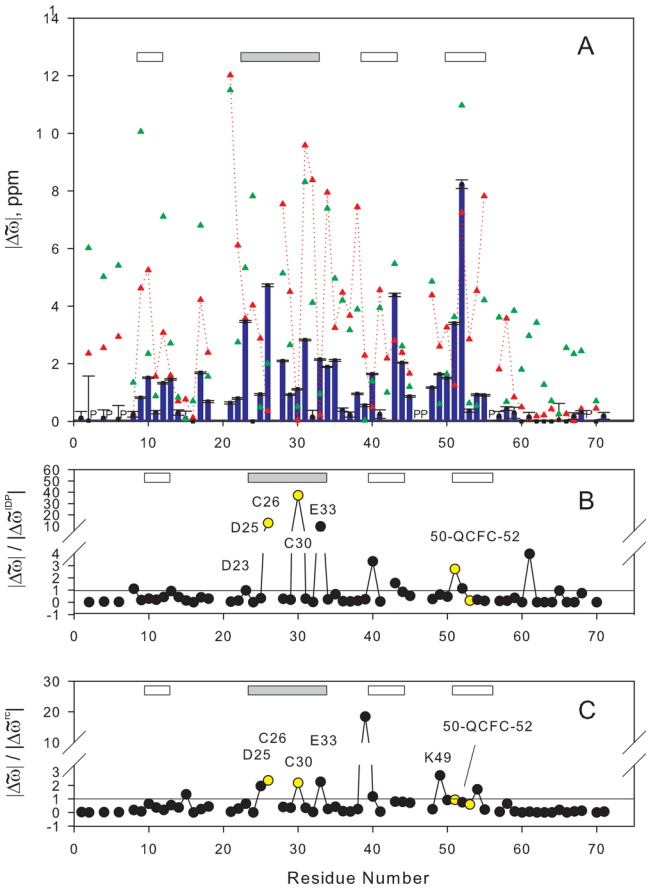

Figure 4. Chemical shifts report on structure of the excited state. (A) The backbone ^{15}N chemical shifts differences between the Sd5 excited and ground states ($\Delta\varpi$) as a function of residue number (blue bars). We have not attempted measurements of ^{15}N $\Delta\varpi$ signs; therefore, absolute values of the chemical shift differences are compared. Red triangles show the differences between experimental ^{15}N chemical shifts of the ground state (BRMB no. 16666) and the intrinsically disordered protein (IDP) chemical shifts predicted for the Sd5 sequence ($\Delta\varpi^{IDP}$) as described by Tamiola et al. (2010),[37] while green triangles show the differences between chemical shifts of the ground state and the random coil chemical shifts calculated as described in Schwarzinger et al.[38,39] ($\Delta\varpi^{rc}$). Seven prolines in Sd5, for which ^{15}N CPMG dispersions could not be measured, are marked with "P". (B) $\Delta\varpi/\Delta\varpi^{IDP}$ and (C) $\Delta\varpi/\Delta\varpi^{rc}$ ratios as a function of residue number (where the yellow circles denote cystine residues). The secondary structure diagram based on the Sd5 structure is shown at the top, where the α-helix is shown as a gray bar and β-strands are shown as open rectangles.

absolute values of the chemical shift differences between the Sd5 ground and excited states extracted from ^{15}N CPMG RD data, $|\Delta\varpi|$, and their comparison with the differences between experimental chemical shifts of the ground state and a neighbor-corrected IDP chemical shifts for the Sd5 sequence[37] ($|\Delta\varpi^{IDP}|$) or predicted random coil chemical shifts ($|\Delta\varpi^{rc}|$).[38,43] (See also Figures S2 and S3.) Here, the random coil chemical shifts were obtained from model peptides under denaturing conditions,[38] while the neighbor-corrected IDP chemical shifts were obtained from a library of assigned IDPs.[37] All secondary structure elements of Sd5 are involved in conformational exchange and display the backbone ^{15}N chemical shift differences of up to 8 ppm (e.g., Phe 52). Most prominent chemical shift changes upon transition to the excited state occur in the α-helix and in the β-strand 3 cross-linked by the two disulfide bridges. These are the two Sd5 regions with ^{15}N chemical shift changes $\Delta\varpi$ upon transition to the excited state for some residues of the order or greater than $\Delta\varpi^{rc}$ or $\Delta\varpi^{IDP}$, suggesting a significant reorganization of these secondary structure elements. While most residues from the β-strand 3 display $\Delta\varpi \sim \Delta\varpi^{rc}$, four residues from the α-helix (Asp25, Cys26, Cys30, and Glu33) exhibit $\Delta\varpi$ greater than $\Delta\varpi^{rc}$ (Figure 4C) or $\Delta\varpi^{IDP}$ (Figure 4B). Such chemical shift changes in the Sd5 α-helix point to a major conformational rearrangement such as α- to β-transition, in which the Sd5 α-helix adopts an extended conformation or other major reorganization of the Sd5 secondary structure (although ^{15}N chemical shift data are not conclusive and need to be validated by chemical shift changes for other nuclei). The observation of large chemical shift changes for the Sd5 α-helix (as compared to chemical shift changes $\Delta\varpi^{rc}$ and $\Delta\varpi^{IDP}$ expected for protein unfolding) is also important because it implies a significant rearrangement of the α-helix relative to the β-sheet in the excited state, providing an explanation for a global conformational exchange in Sd5 involving all secondary structure elements.

DOI: 10.1021/acs.biochem.8b00753
Biochemistry 2018, 57, 5797−5806

Previous reports suggest that a chemokine Lymphotactin (Ltn), which adopts a typical chemokine fold with an α-helix packed against 3-stranded β-sheet, can also adopt an alternative all-β arrangement, in which an α-helix converts into an extended structure.[44] The chemokine native structure is similar to the structure of defensins, yet the two classes of protein have different topologies ($\beta\beta\beta\alpha$ for chemokines and $\beta\alpha\beta\beta$ for defensins). The observation of an alternative all-β fold for a related class of protein provides an additional indication that conformational exchange in Sd5 might involve transitions to a low-populated conformer where the α-helix converts to an extended β-like structure.

Exchange Process in the Sd5 Involves Rearrangement of Surface-Exposed Side Chains. Our previous studies[3,13,15] revealed fundamental differences between the structural organization of Sd5 and regular globular proteins. The Sd5 structure is held together by four conserved disulfide bridges and lacks an extensive hydrophobic core characteristic of water-soluble globular proteins. Instead, the structure is stabilized by contacts among surface-exposed polar and hydrophobic side chains. Figure 5A (red) shows all hydrophobic residues in Sd5 with a Kyte−Doolittle hydrophobicity index greater than 0. Remarkably, all of these residues have a significant surface exposure.

An indirect way of estimating relative contributions of interactions mediated by polar and hydrophobic surface-exposed residues to Sd5 stabilization is by analysis of long-range NOEs used for its NMR structure calculation.[15] The NOE contact map of Sd5 (Figure S4) shows that most long-range NOEs in Sd5 are among surface-exposed polar/charged amino acid side chains. Only three groups of NOEs are among hydrophobic residues that form small hydrophobic clusters on the Sd5 surface (Figure S4, red) shown in Figure 5B−D. Thus, nonpolar contacts at the α-helix surface involve side chains of Met24, Ala28 and Ala29, and Val31 (Figure 5B). Another example is the interaction between the exposed side chains of Pro56 and Ile8 (Figure 5D). We have also observed many contacts among polar/charged residues such as Thr, Tyr, Lys, Arg, Glu, and Gln that can make hydrophobic contacts through their aliphatic chains, aromatic rings, and/or methyl groups. Examples include a contact between the aromatic ring of Tyr16 and methyl group of Ala29 (Figure 5B) and a sandwich formed by Phe52 ring flanked by aliphatic chains of Gln50 on one side and Lys10 on the other side (Figure 5C). These kinds of hydrophobic contacts are the most prevalent on the Sd5 surface.

The backbone ^{15}N CPMG RD measurements revealed significant conformational changes in Sd5 accompanied by large ^{15}N chemical shift changes in all parts of the protein (Figure 4). The observed chemical shift changes are consistent with a major reorganization of the Sd5 secondary structure such as α- to β-transition of the Sd5 α-helix. It is inevitable that such a change is accompanied by a significant rearrangement of the Sd5 surface-exposed side chains. Since contacts between the exposed side chains play a role in stabilization of the Sd5 structure, rearrangement of these contacts in the excited state (along with secondary structure reorganization) may explain the observed enthalpy change upon transition to the excited state (Figure 2E). On the other hand, side-chain rearrangement may also create more extensive hydrophobic clusters on the Sd5 surface, resulting in a decrease in accessible surface area of the Sd5 in the excited state suggested by the m value changes obtained from CPMG RD data measured at different denaturant concentrations (Figure 3E). It is conceivable that this side-chain rearrangement may play a role in the Sd5 function by creating new interaction interfaces, which confer Sd5 the ability to bind multiple partners.

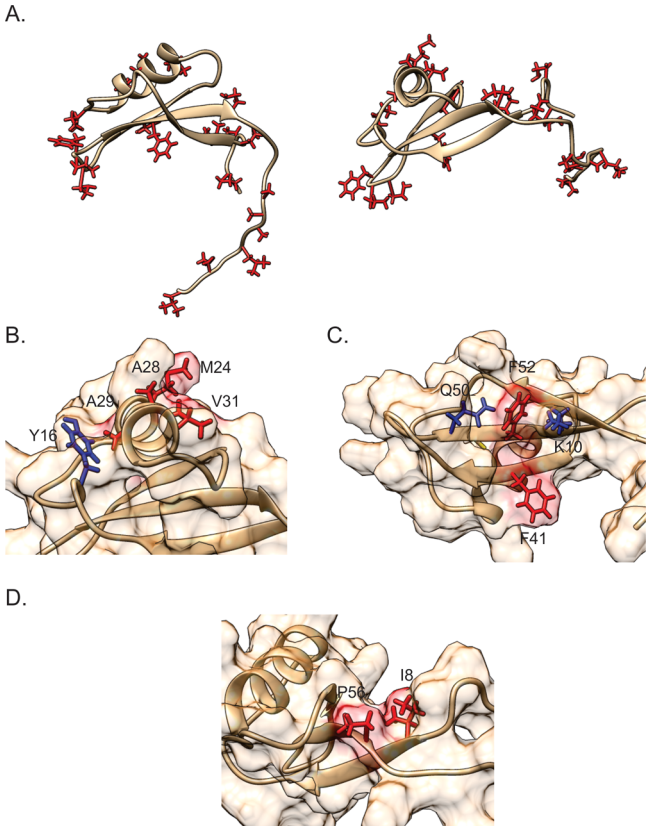

Figure 5. (A) Ribbon representation of the Sd5 structure showing side chains of all hydrophobic residues with a Kyte−Doolittle hydrophobicity index[45] greater than 0. Note that all hydrophobic residues in Sd5 are surface-exposed. (B) Close-up view of the α-helix showing surface-exposed side chains of M24, A28, A29, and V31 (red). Shown in blue is Tyr16, which forms a contact with Ala29 important for protein stabilization. (C) Close-up view of the surface-exposed side chains of Phe52 and Phe41; Phe52 ring is flanked on both sides by chains of Lys10 and Gln50 (blue). (D) Close-up view of interactions between Ile8 and Pro56 at the protein surface. These interactions are corroborated by long-range NOEs (Figure S2) and are the closest Sd5 gets to a hydrophobic core.

DISCUSSION

Plant defensins Sd5[15] and Psd1[13,14] share the same fold and the ability to bind fungal membrane glucocerebroside CMH, thus playing a central role in cellular antimicrobal defense. Despite their structural and functional similarity, their binding site for CMH and conformational dynamics are diverse. In contrast to Psd1, the Sd5 defensin possesses a long intrinsically disordered C-terminal part and a shorter disordered N-terminus. Psd1 binding site for CMH is located in the α1-β2 loop, which displays μs-ms time-scale conformational exchange, pointing to a conformational selection mechanism for the CMH recognition.[13] Sd5 also specifically binds CMH, yet using a different site encompassing the end of α-helix 1 and α1-β2 loop. Here, conformational selection may also play a role, since these residues are in the α-helix region undergoing large-scale conformational rearrangements observed in this work. The above-mentioned differences may be explained by

DOI: 10.1021/acs.biochem.8b00753
Biochemistry 2018, 57, 5797−5806

the fact that Sd5 emerged much later in the defensin evolution. Thus, evolutionary analysis suggests that Psd1 evolved around 80 mya, while Sd5 diverged only about 7 mya.[3]

All plant defensins share the same cysteine-stabilized fold.[10,16] However, the primary sequence diversity in the defensin family is extremely high with cysteines being the only conserved residues required to maintain the CS$\alpha\beta$ fold.[4] This fold is also present in toxins and enzyme inhibitors.[46] Structural analysis suggests that, similar to Sd5, all of these disulfide-stabilized proteins lack a typical hydrophobic core present in globular proteins and instead are stabilized by contacts between surface-exposed hydrophobic and polar residues. The high sequence diversity in proteins sharing the CS$\alpha\beta$ fold and their "inside-out" arrangement, which allows exposing multiple hydrophobic side chains, reveals an evolutionary mechanism to create versatile binding sites making it possible for proteins within the same family to fulfill diverse and different functions. Furthermore, the example of Sd5 and Psd1 plant defensins suggests that these proteins evolved different side-chain arrangements, which enable them to bind the same partner via different interaction interfaces, i.e., to fulfill the same function in a number of different ways.

The Sd5 defensin provides a remarkable example of evolution of the CS$\alpha\beta$ fold because it can exist in two alternative well-ordered conformational states with significantly different backbone and side-chain arrangements. Here we have shown that the native state of the Sd5, which has a typical CS$\alpha\beta$ fold, undergoes a millisecond time-scale interconversion with an alternative conformational state, which is enthalpically less favorable and yet is more compact than the native state. The backbone ^{15}N chemical shift changes obtained from CPMG RD data suggest that the Sd5 α-helix undergoes a significant rearrangement in the excited state, possibly transforming into an extended β-structure. It worth mentioning in this respect that a chemokine Lymphotactin (Ltn), which has an α/β fold resembling the defensin structure (albeit having different topology), can also adopt an alternative but functional all-β dimeric fold. Therefore, Ltn provides a rare example of a metamorphic protein that can adopt two alternative folds fulfilling different functions.[47] Our results suggest that the Sd5 defensin also belongs to a class of metamorphic proteins that can exist in two well-ordered yet structurally distinct (potentially multifunctional) conformational states.

We propose that the versatility of the CS$\alpha\beta$ fold, which enables functional diversity within the defensin family and allows individual defensins to fulfill multiple functions, is the reason why this fold is so ancestral and prevalent. It enables, in an energetically favorable way, to expose and rearrange hydrophobic residues at the protein surface, providing an evolutionary mechanism to create diverse specific binding sites. The present work unraveled thermodynamics and structural features of the Sd5 excited state based on ^{15}N chemical shifts derived from relaxation dispersion data, providing first experimental evidence of the link between conformational dynamics and functional diversity of CS$\alpha\beta$ proteins. There are ample opportunities for a further investigation of small and highly cross-linked proteins, including forthcoming structure determination of the Sd5 excited state based on the nearly complete set of the backbone chemical shifts.

■ ASSOCIATED CONTENT

Supporting Information

The Supporting Information is available free of charge on the ACS Publications website at DOI: 10.1021/acs.biochem.8b00753.

^{15}N CPMG RD data fits, thermodynamic parameters, ^{15}N CPMG RD profiles, chemical shift differences between "excited" and ground states of Sd5 ($\Delta\varpi$), and contact maps of Sd5 based on long-range NOEs used for Sd5 structure determination (PDF)

■ AUTHOR INFORMATION

Corresponding Authors

*E-mail: korzhniev@uchc.edu.

*E-mail: falmeida@bioqmed.ufrj.br.

ORCID

Fabio C. L. Almeida: 0000-0001-6046-7006

Funding

The work presented here was funded by FAPERJ grants 215141, 210361, and 204432 awarded to F.C.L.A., CNPq grants 209306/2013-2 and 457773/2014-6 awarded to F.C.L.A., and FINEP grant 0267/16 awarded to F.C.L.A.

Notes

The authors declare no competing financial interest.

■ ACKNOWLEDGMENTS

We thank the facilities of Centro Nacional de Ressonância Magnética Nuclear (CNRMN) for the NMR time.

■ REFERENCES

(1) Boehm, T., Iwanami, N., and Hess, I. (2012) Evolution of the immune system in the lower vertebrates. *Annu. Rev. Genomics Hum. Genet. 13*, 127−49.

(2) Flajnik, M. F., and Du Pasquier, L. (2004) Evolution of innate and adaptive immunity: can we draw a line? *Trends Immunol. 25*, 640−4.

(3) De-Paula, V. S., Razzera, G., Medeiros, L., Miyamoto, C. A., Almeida, M. S., Kurtenbach, E., Almeida, F. C. L., and Valente, A. P. (2008) Evolutionary relationship between defensins in the Poaceae family strengthened by the characterization of new sugarcane defensins. *Plant Mol. Biol. 68*, 321−335.

(4) Gachomo, E. W., Jimenez-Lopez, J. C., Kayodé, A. P. P., Baba-Moussa, L., and Kotchoni, S. O. (2012) Structural characterization of plant defensin protein superfamily. *Mol. Biol. Rep. 39*, 4461−9.

(5) Jannoo, N., Grivet, L., Chantret, N., Garsmeur, O., Glaszmann, J. C., Arruda, P., and D'Hont, A. (2007) Orthologous comparison in a gene-rich region among grasses reveals stability in the sugarcane polyploid genome. *Plant J. 50*, 574−585.

(6) Franco, O. L. (2011) Peptide promiscuity: an evolutionary concept for plant defense. *FEBS Lett. 585*, 995−1000.

(7) Silverstein, K. a T., Moskal, W. a, Wu, H. C., Underwood, B. a, Graham, M. a, Town, C. D., and VandenBosch, K. a. (2007) Small cysteine-rich peptides resembling antimicrobial peptides have been under-predicted in plants. *Plant J. 51*, 262−80.

(8) Silverstein, K. A. T., Graham, M. A., Paape, T. D., and Vandenbosch, K. A. (2005) Genome Organization of More Than 300 Defensin-Like Genes in Arabidopsis 1 [w]. *Plant Physiol. 138*, 600−610.

(9) Wong, J. H., Xia, L., and Ng, T. B. (2007) A review of defensins of diverse origins. *Curr. Protein Pept. Sci. 8*, 446−59.

(10) Thomma, B. P. H. J., Cammue, B. P. A., and Thevissen, K. (2003) Mode of action of plant defensins suggests therapeutic potential. *Curr. Drug Targets: Infect. Disord. 3*, 1−8.

DOI: 10.1021/acs.biochem.8b00753
Biochemistry 2018, 57, 5797−5806

(11) Lacerda, A. F., Vasconcelos, E. a R., Pelegrini, P. B., and Grossi de Sa, M. F. (2014) Antifungal defensins and their role in plant defense. *Front. Microbiol. 5*, 116.
(12) Lobo, D. S., Pereira, I. B., Fragel-Madeira, L., Medeiros, L. N., Cabral, L. M., Faria, J., Bellio, M., Campos, R. C., Linden, R., and Kurtenbach, E. (2007) Antifungal Pisum sativum defensin 1 interacts with Neurospora crassa cyclin F related to the cell cycle. *Biochemistry 46*, 987−96.
(13) de Medeiros, L. N., Angeli, R., Sarzedas, C. G., Barreto-Bergter, E., Valente, A. P., Kurtenbach, E., and Almeida, F. C. L. (2010) Backbone dynamics of the antifungal Psd1 pea defensin and its correlation with membrane interaction by NMR spectroscopy. *Biochim. Biophys. Acta, Biomembr. 1798*, 105−13.
(14) Almeida, M. S., Cabral, K. M. S., Kurtenbach, E., Almeida, F. C. L., and Valente, A. P. (2002) Solution structure of Pisum sativum defensin 1 by high resolution NMR: plant defensins, identical backbone with different mechanisms of action. *J. Mol. Biol. 315*, 749−57.
(15) de Paula, V. S., Razzera, G., Barreto-Bergter, E., Almeida, F. C. L., and Valente, A. P. (2011) Portrayal of complex dynamic properties of sugarcane defensin 5 by NMR: multiple motions associated with membrane interaction. *Structure 19*, 26−36.
(16) Thevissen, K., Warnecke, D. C., François, I. E. J. a, Leipelt, M., Heinz, E., Ott, C., Zähringer, U., Thomma, B. P. H. J., Ferket, K. K. a, and Cammue, B. P. a. (2004) Defensins from insects and plants interact with fungal glucosylceramides. *J. Biol. Chem. 279*, 3900−5.
(17) Aerts, A. M., Bammens, L., Govaert, G., Carmona-Gutierrez, D., Madeo, F., Cammue, B. P. A., and Thevissen, K. (2011) The Antifungal Plant Defensin HsAFP1 from Heuchera sanguinea Induces Apoptosis in Candida albicans. *Front. Microbiol. 2*, 47.
(18) De Paula, V. S., Gomes, N. S. F., Lima, L. G., Miyamoto, C. A., Monteiro, R. Q., Almeida, F. C. L., and Valente, A. P. (2013) Structural Basis for the Interaction of Human β-Defensin 6 and Its Putative Chemokine Receptor CCR2 and Breast Cancer Microvesicles. *J. Mol. Biol. 425*, 4479−4495.
(19) Vriens, K., Cammue, B. P. A., and Thevissen, K. (2014) Antifungal plant defensins: Mechanisms of action and production. *Molecules 19*, 12280−12303.
(20) Valente, A., de Paula, V., and Almeida, F. (2013) Revealing the Properties of Plant Defensins through Dynamics. *Molecules 18*, 11311−11326.
(21) Mittermaier, A. K., and Kay, L. E. (2009) Observing biological dynamics at atomic resolution using NMR. *Trends Biochem. Sci. 34*, 601−11.
(22) Henzler-Wildman, K., and Kern, D. (2007) Dynamic personalities of proteins. *Nature 450*, 964−972.
(23) Cruzeiro-Silva, C., Gomes-Neto, F., Machado, L. E. S. F., Miyamoto, C. A., Pinheiro, A. S., Correa-Pereira, N., de Magalhães, M. T. Q., Valente, A. P., and Almeida, F. C. L. (2014) Hydration and conformational equilibrium in yeast thioredoxin 1: implication for H+ exchange. *Biochemistry 53*, 2890−2902.
(24) Valente, A. P., Miyamoto, C. A., and Almeida, F. C. L. (2006) Implications of protein conformational diversity for binding and development of new biological active compounds. *Curr. Med. Chem. 13*, 3697−3703.
(25) Korzhnev, D. M., Religa, T. L., Banachewicz, W., Fersht, A. R., and Kay, L. E. (2010) A Transient and Low-Populated Protein-Folding Intermediate at Atomic Resolution. *Science (Washington, DC, U. S.) 329*, 1312−1316.
(26) Hansen, A. L., Lundström, P., Velyvis, A., and Kay, L. E. (2012) Quantifying Millisecond Exchange Dynamics in Proteins by CPMG Relaxation Dispersion NMR Using Side-Chain (1)H Probes. *J. Am. Chem. Soc. 134*, 3178−89.
(27) Korzhnev, D. M., Orekhov, V. Y., and Kay, L. E. (2005) Off-resonance R(1rho) NMR studies of exchange dynamics in proteins with low spin-lock fields: an application to a Fyn SH3 domain. *J. Am. Chem. Soc. 127*, 713−21.
(28) Hansen, D. F., Vallurupalli, P., and Kay, L. E. (2008) An improved 15N relaxation dispersion experiment for the measurement of millisecond time-scale dynamics in proteins. *J. Phys. Chem. B 112*, 5898−904.
(29) McConnell, H. M. (1958) Reaction Rates by Nuclear Magnetic Resonance. *J. Chem. Phys. 28*, 430−1.
(30) Korzhnev, D. M., Salvatella, X., Vendruscolo, M., Di Nardo, A. A., Davidson, A. R., Dobson, C. M., and Kay, L. E. (2004) Low-populated folding intermediates of Fyn SH3 characterized by relaxation dispersion NMR. *Nature 430*, 586−90.
(31) Korzhnev, D. M., Religa, T. L., Lundström, P., Fersht, A. R., and Kay, L. E. (2007) The folding pathway of an FF domain: characterization of an on-pathway intermediate state under folding conditions by (15)N, (13)C(alpha) and (13)C-methyl relaxation dispersion and (1)H/(2)H-exchange NMR spectroscopy. *J. Mol. Biol. 372*, 497−512.
(32) Korzhnev, D. M., Bezsonova, I., Evanics, F., Taulier, N., Zhou, Z., Bai, Y., Chalikian, T. V., Prosser, R. S., and Kay, L. E. (2006) Probing the Transition State Ensemble of a Protein Folding Reaction by Pressure-Dependent NMR Relaxation Dispersion. *J. Am. Chem. Soc. 128*, 5262−5269.
(33) Choy, W.-Y., Zhou, Z., Bai, Y., and Kay, L. E. (2005) An 15N NMR spin relaxation dispersion study of the folding of a pair of engineered mutants of apocytochrome b562. *J. Am. Chem. Soc. 127*, 5066−72.
(34) Hagen, S. J., Hofrichter, J., Szabo, A., and Eaton, W. A. (1996) Diffusion-limited contact formation in unfolded cytochrome c: estimating the maximum rate of protein folding. *Proc. Natl. Acad. Sci. U. S. A. 93*, 11615−11617.
(35) Korzhnev, D. M., Neudecker, P., Mittermaier, A., Orekhov, V. Y., and Kay, L. E. (2005) Multiple-Site Exchange in Proteins Studied with a Suite of Six NMR Relaxation Dispersion Experiments: An Application to the Folding of a Fyn SH3 Domain Mutant. *J. Am. Chem. Soc. 127*, 15602−15611.
(36) Neudecker, P., Korzhnev, D. M., and Kay, L. E. (2006) Assessment of the effects of increased relaxation dispersion data on the extraction of 3-site exchange parameters characterizing the unfolding of an SH3 domain. *J. Biomol. NMR 34*, 129−35.
(37) Tamiola, K., Acar, B., and Mulder, F. A. A. (2010) Sequence-specific random coil chemical shifts of intrinsically disordered proteins. *J. Am. Chem. Soc. 132*, 18000−18003.
(38) Schwarzinger, S., Kroon, G. J., Foss, T. R., Wright, P. E., and Dyson, H. J. (2000) Random coil chemical shifts in acidic 8 M urea: implementation of random coil shift data in NMRView. *J. Biomol. NMR 18*, 43−8.
(39) Merutka, G., Dyson, H. J., and Wright, P. E. (1995) Random coil" 1H chemical shifts obtained as a function of temperature and trifluoroethanol concentration for the peptide series GGXGG. *J. Biomol. NMR 5*, 14−24.
(40) Korzhnev, D. M., Neudecker, P., Zarrine-Afsar, A., Davidson, A. R., and Kay, L. E. (2006) Abp1p and Fyn SH3 Domains Fold through Similar Low-Populated Intermediate States [?] *Biochemistry 45*, 10175−10183.
(41) Fersht, A. (1999) Structure and mechanism in protein science: A guide to enzyme catalysis and protein folding. *Lavoisier.Fr*.
(42) Myers, J. K., Pace, C. N., and Scholtz, J. M. (1995) Denaturant m values and heat capacity changes: Relation to changes in accessible surface areas of protein unfolding. *Protein Sci. 4*, 2138−2148.
(43) Wishart, D. S., Sykes, B. D., and Richards, F. M. (1992) The chemical shift index: a fast and simple method for the assignment of protein secondary structure through NMR spectroscopy. *Biochemistry 31*, 1647−1651.
(44) Tuinstra, R. L., Peterson, F. C., Kutlesa, S., Elgin, E. S., Kron, M. a, and Volkman, B. F. (2008) Interconversion between two unrelated protein folds in the lymphotactin native state. *Proc. Natl. Acad. Sci. U. S. A. 105*, 5057−5062.
(45) Kyte, J., and Doolittle, R. F. (1982) A simple method for displaying the hydropathic character of a protein. *J. Mol. Biol. 157*, 105−32.

DOI: 10.1021/acs.biochem.8b00753
Biochemistry 2018, 57, 5797−5806

(46) Yount, N. Y., and Yeaman, M. R. (2004) Multidimensional signatures in antimicrobial peptides. *Proc. Natl. Acad. Sci. U. S. A. 101*, 7363−8.
(47) Murzin, A. G. (2008) Biochemistry. Metamorphic proteins. *Science 320*, 1725−1726.

DOI: 10.1021/acs.biochem.8b00753
Biochemistry 2018, 57, 5797−5806